CO_2 and O_2 oxidized 2.7 Ga micrometeorites in two stages suggesting a >32% CO_2 atmosphere

G. Huang[1,2]*, J. K. Eager[3], N. J. Mayne[3], D. Cui[1], J. Manners[2,4], E. Hebrard[3], Z. Liu[1], and T. M. Lenton[2]

[1]*Department of Earth System Science, Tsinghua University, Beijing 100084, China.*

[2]*Global Systems Institute, University of Exeter, Exeter EX4 4QE, UK.*

[3]*Astrophysics Group, University of Exeter, Exeter EX4 4QL, UK.*

[4]*Met Office, FitzRoy Road, Exeter, EX1 3PB, UK*

**Corresponding author. Email: hg17@mails.tsinghua.edu.cn ;*

ABSTRACT

It is widely accepted that atmospheric pO_2 <1 ppm before the Great Oxidation Event. Yet a recent study found fossil micrometeorites (MMs) containing the oxidized iron species wüstite (FeO) and magnetite (Fe_3O_4) formed 2.7 billion years ago (Ga). How these MMs became oxidized is uncertain. Abundant O_2 in the upper atmosphere and iron oxidation by CO_2 have been suggested. However, photochemical reactions cannot produce sufficient O_2, and oxidation by CO_2 can only produce FeO, each individually failing to explain the formation of Fe_3O_4-only MMs. Using an oxidation model of iron MMs including photochemistry, we show that a >32% CO_2 Archean atmosphere and different entry angles can generate the Fe_3O_4-only and Fe-FeO mixed composition MMs that have been discovered. Oxidation happens in two stages: by CO_2 under brief melting, then by O_2. Our results challenge existing constraints on Earth's atmospheric CO_2 concentration at 2.7 Ga and support a warm Late Archean despite the

23 ‘faint young Sun’.

24 **INTRODUCTION**

25 Whether the Archean atmosphere contained significant oxygen (O_2) has been a topic of
26 considerable debate. Cloud (1972) first established the case for a ‘Great Oxidation
27 Event’ (GOE) having taken place around 2.3 billion years ago (Ga) on the basis of
28 changes in the redox state of iron and sulfur sedimentary deposits and of ancient soils
29 (paleosols), showing a lack of oxidation of pyrite and uraninite beforehand and
30 extensive oxidation afterwards. Kasting (1987, 1993) provided further modeling
31 support for very low O_2 levels in the Archean atmosphere. Ohmoto (1996) challenged
32 this view, arguing that free O_2 existed in the Archean. However, the argument swung
33 decisively in favor of very low O_2 with the discovery of the mass-independent fraction
34 of sulfur isotopes (MIF-S) prior to the Great Oxidation (Farquhar et al., 2000). This
35 requires the absence of an ozone layer and of sulfate in the ocean – requiring O_2 mixing
36 ratios $<10^{-5}$ of the present atmospheric level (PAL, 0.21 atm) (Pavlov and Kasting,
37 2002). The GOE is now widely accepted and interpreted as O_2 rising above 10^{-5} PAL
38 in the interval 2.4 – 2.1 Ga (Gregory et al., 2021). This divides Earth’s atmospheric
39 history into two parts: pre-GOE (reducing atmosphere) and post-GOE (oxidizing
40 atmosphere).

41 The recent discovery of oxidized fossil micrometeorites (MMs) formed at 2.7 Ga
42 (Tomkins et al., 2016) is therefore surprising. To explain how these fossil MMs were
43 oxidized, Tomkins et al. (2016) proposed that the upper atmospheric O_2 content above
44 75 km at this time during the Late Archaean might have been close to 1 PAL. If correct,

45 this interpretation of the oxidized fossil MMs would change our understanding of the
46 ancient atmosphere. But a key question must be resolved regarding the source of the
47 upper atmospheric oxidizing power, given established constraints that the O_2
48 concentration was very low in the troposphere. Tomkins et al. (2016) favor O_2 as the
49 oxidant, generated by the photolysis of CO_2, but they also show in their Extended Data
50 Figure 5 that CO_2 could have directly oxidized the MMs, albeit at a slower rate that is
51 hard to reconcile with the data.
52 Recently, Lehmer et al. (2020) modeled the trajectory of MMs through the atmosphere,
53 combined with a treatment of the chemical kinetics to propose that CO_2 rather than O_2
54 was responsible for the oxidation of the MMs. This implies a Late Archean atmosphere
55 with >70% CO_2 mixing ratio. However, Lehmer et al. (2020) used the 'solution
56 chemistry' method to obtain the Fe-CO_2 reaction rate: Where a virtual volume is
57 assumed and CO_2 concentration calculated, leading to an incorrect estimation because
58 the Fe-CO_2 reaction is a solid-gas or liquid-gas reaction in which the CO_2 partial
59 pressure should be applied instead. By applying a one-dimensional photochemical
60 model, Payne et al. (2020) claimed that an Archean atmosphere containing at least 23%
61 CO_2 could have produced the MMs found by Tomkins et al. (2016). However, Payne
62 et al. (2020) did not consider that the temperature change of MMs could affect the
63 reaction rate, which is why their required CO_2 fraction is much lower than the value
64 argued by Lehmer et al. (2020). Explanations of the oxidized MMs formed at 2.7 Ga
65 need to consider both the trajectory of MMs and the atmospheric chemistry at that time,
66 whereas previous studies neglect either motion or photochemistry.

Moreover, since CO_2 is not an efficient oxidant, it is difficult to produce magnetite through the Fe-CO_2 reaction. The formation of iron oxides is described by *Eq (1-4)* (Abuluwefa et al., 1997; Garnaud and Rapp, 1977; Himmel et al., 1953; Young, 2008).

$$Fe \xrightarrow{Step\ 1} FeO \xrightarrow{Step\ 2} Fe_3O_4, \quad (1)$$

$$Fe + CO_2 \rightarrow FeO + CO, \quad (2)$$

$$3FeO + CO_2 \rightarrow Fe_3O_4 + CO, \quad (3)$$

$$6FeO + O_2 \rightarrow Fe_3O_4. \quad (4)$$

If CO_2 is considered as the oxidant, Step 1 and Step 2 in *Eq (1)* would be *Eq (2)* and *Eq (3)*, respectively. However, existing experiments on Fe-CO_2 reactions do not show CO_2 can fully oxidize Fe to Fe_3O_4 (Abuluwefa et al., 1997; Shao et al., 2020), implying the production of Fe_3O_4-only MMs via *Eq (3)* is implausible and the argument that MMs were oxidized by CO_2 alone cannot explain the formation of the Fe_3O_4-only particles found by Tomkins et al. (2016). Since the oxidation path by CO_2 could not produce Fe_3O_4-only MMs, another strong oxidant must have played a role in Step 2 of *Eq (1)*.

In this study, we favor O_2 (*Eq 4*) from the photolysis of CO_2, which in the deeper atmosphere oxidized FeO to generate Fe_3O_4. Zahnle and Buick (2016) suggested that the photolysis of CO_2 should have produced a corresponding amount of CO, leaving the atmosphere no more oxidizing overall than CO_2. However, the reduction of Fe_3O_4 by CO is depressed when the temperature is below 870K (Corbari and Fruehan, 2010). Here we propose that the Fe_3O_4-only MMs experienced two oxidation stages: 1) Particle melting and oxidation by CO_2 to form FeO, and 2) Particle oxidation by O_2 to Fe_3O_4. In this study, we advance previous studies by considering both motion and

atmospheric photochemistry. We use an atmospheric entry model of iron MMs and a one-dimensional photochemical model to simulate the oxidation of MMs formed at 2.7 Ga. Our results show that Fe_3O_4-only and Fe-FeO mixed MMs with radii ranging from 5 to 25 micrometers (μm), as found by Tomkins et al. (2016), could both be predicted in an atmosphere with >32% CO_2 but 1×10^{-8} ground-level O_2.

METHOD

Micrometeorite Oxidation Model

Love and Brownlee (1991) first proposed a numerical model containing equations of motion, temperature change, and evaporation to describe MMs' trajectories and radii change in the atmosphere. Based on Love and Brownlee (1991), Genge (2016) simulated the composition change of MMs considering oxidation by O_2. Lehmer et al. (2020) developed another version in which CO_2 oxidizes MMs. However, neither Genge (2016) nor Lehmer et al. (2020) considered that the concentrations of O_2 and CO_2 change with altitude due to atmospheric photochemistry, leading to inaccuracies in their results. Payne et al. (2020) firstly applied photochemical model results to explain the 2.7 Ga oxidized MMs, but lack of treatment of the changes in temperature of the MMs and chemical kinetics between iron and air making their estimation less convincing.

To more accurately simulate how MMs were oxidized, a treatment of the photochemistry must be integrated with a model of the motion or trajectory. Hence, we have developed a Micrometeorites Oxidation Model Including Photochemistry (MOMIP), which applies the photochemical model results to the oxidation of MMs.

The MOMIP contains five modules: motion, thermal equilibrium, chemical oxidation, thermal evaporation, and atmospheric photochemistry, which fully consider the changes of velocity, temperature, composition, volume, density, and other properties. The diversity of chemical modules is also enhanced in the MOMIP by considering both O_2-Fe and CO_2-Fe reactions.

The MOMIP's motion module (*Eq 5*) is based on Love and Brownlee (1991), while the heat (q) change, following Genge (2016), is treated through thermal balance (*Eq 6-11*).

$$d\mathbf{v} = (-3\rho_{air}/4\rho_{particle} \cdot v^2/r + \mathbf{g})\, dt, \quad (5)$$

$$dq = (P_{\_collision} + P_{\_evaporation} + P_{\_emission} + P_{\_redox})\, dt, \quad (6)$$

$$P_{\_collision} = \rho_{air}\pi r^2 v^3/2, \quad (7)$$

$$P_{\_evaporation} = -dm_{ev}/dt \cdot L_v, \quad (8)$$

$$P_{\_emission} = -4\varepsilon\sigma\pi r^2 T^4, \quad (9)$$

$$P_{\_redox} = \Sigma\Delta H_{ox} dm_{ox}/dt + \Sigma\Delta H_{re} dm_{re}/dt, \quad (10)$$

$$dq/dt = c_p \cdot dT/dt. \quad (11)$$

Where $\mathbf{v}$ (vector), *v, and* $\hat{v}$ are the particle's velocity, velocity magnitude, and velocity direction respectively, $\mathbf{g}$ (vector) is the gravitational acceleration, $\rho_{particle}$ is particle's mass density, ρ_{air} is the mass density of encountered air, r is particle's radius, and dt is the time interval, 10^{-8} s in the first timestep and adjusted according to the velocity. $P_{\_collision}$, $P_{\_evaporation}$, $P_{\_emission}$, $P_{\_redox}$ are the heating flux of collision with air, evaporation, emission, and redox, respectively. The latent heat of evaporation for both FeO and Fe (L_v) is given by Genge (2016). ε is particle emissivity, σ is the Stefan-

Boltzmann constant, and T is particle temperature. Constants used in the MOMIP are shown in Table 1. m_{ev}, m_{ox}, and m_{re} are masses that participate in evaporation, oxidation, and reduction, respectively. ΔH_{ox} and ΔH_{re} are the enthalpy of oxidation and reduction, data from NIST Chemistry WebBook database (https://webbook.nist.gov/). c_p is the particle's specific heat, varies as the particle's content changes.

Table 1. Constants used in the MOMIP model.

Constants	**g**	L_v	σ	ε
Value	9.807 m s^{-2}	6×10^6 J kg^{-1}	5.67×10^{-8} W m^{-2} K^{-4}	1

The motion and oxidation of MMs are simulated in the MOMIP through splitting the trajectories to many timesteps. When a timestep of the simulation starts, the MOMIP's motion module calculates the collisions between the simulated MM and air molecules based on the iron particle's velocity and position from the last timestep. Collisions determine the particle's deceleration and hence affect the trajectory and altitude. Next, the surrounding air properties (air compositions and density) are imported from the photochemical model according to the MM's altitude. The chemical module then calculates the MM's mass and composition changes due to reactions based on the surrounding air properties, the MM's temperature, and the chemical reaction rate constants from interfacial reaction theories of metal (Abuluwefa et al., 1997; Himmel et al., 1953; Smirnov, 2008; Vicentini et al., 2020; Young, 2008). After chemical reactions, the MM's mass loss due to thermal evaporation is derived. The thermal equilibrium module thereupon outputs the MM's temperature by combining the heat effects of chemical reactions, collisions with air molecules, evaporation, and thermal

emission. At the end of the timestep, the MOMIP calculates the MM's radii based on the mass and composition. Finally, the MM's velocity, position, radii, and temperature are transferred to the next timestep. When the MM reaches the Earth's surface, the MOMIP calculation stops.

Tomkins et al. (2016) found radii of 2.7Ga MMs range from 4.3μm to 25μm but only presented Fe_3O_4-only MMs with radii >5μm. The chemical composition of 4.3μm-radius MM is unpublished. Therefore, iron particles with radii ranging from 5μm to 25μm are simulated in this study.

Photochemical Model

The photochemical effect is considered by using the ATMOS model, which is a coupled one-dimensional photochemical-climate model that simulates the composition of the atmosphere at any time since Earth's formation. ATMOS combines the work of several groups over many years (Arney et al., 2016; Gregory et al., 2021; Kasting and Donahue, 1980; Kasting et al., 1979; Kasting et al., 1983; Pavlov et al., 2001; Ribas et al., 2005; Zahnle et al., 2006; Zahnle, 1986; Zerkle et al., 2012). The photochemical version used in this study is an improved, public version of the model (Arney et al., 2016). In our simulations, ATMOS was modified to make it suitable for 2.7 Ga Earth, including 96 species and 459 chemical reactions, while initial CO_2 content ranges from 10% to 50%. The modeled 100 km-thick atmospheres inside ATMOS are divided into 200 layers with a resolution of 0.5-km grid size, and the solar UV flux is scaled to 2.7 Ga by the Ribas et al. (2005) method.

RESULTS

Figure 1 presents the ATMOS model results for O_2, CO, and CO_2 profiles using different initial CO_2 concentrations (fCO_2). Our photochemical results show that the photolysis of CO_2 can maintain an slightly oxic upper atmosphere. The O_2 in the upper atmosphere mainly exists in the form of atomic oxygen (O) while molecular oxygen (O_2) exists mainly at lower altitudes, so the O_2 content shown in Figure 1 is half of the O content plus the O_2 content ($0.5\times O+O_2$). The profiles of atmospheric compositions are similar to Payne et al. (2020) because the photochemical model employed in that study is similar to the one used here.

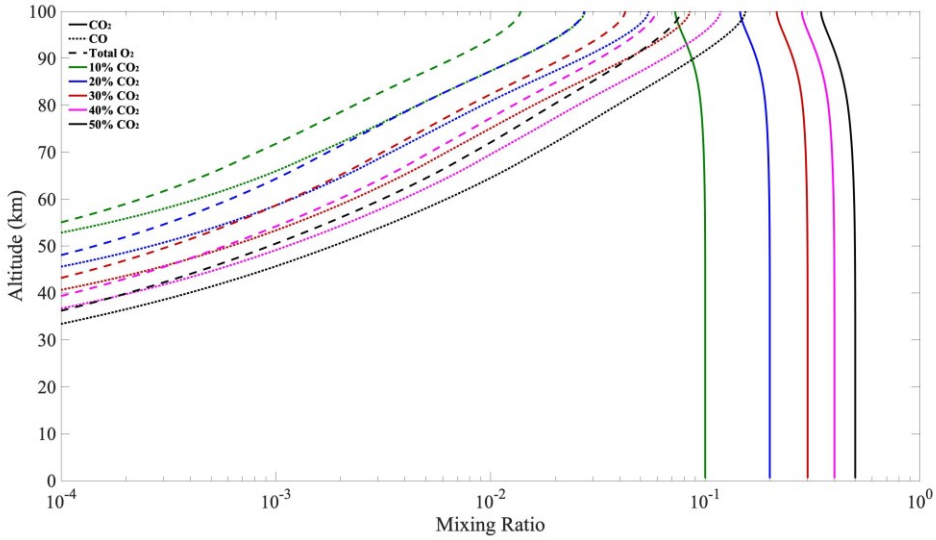

Figure 1. Results of the ATMOS model. Vertical profiles of the mixing ratios of various atmospheric species for five different initial CO_2 compositions. The dashed lines represent the total O_2 mixing ratio ($0.5\times O+O_2$), solid lines the CO_2, and dotted lines CO. Coloured lines correspond to cases with different fCO_2.

In all five different initial CO_2 cases of Figure 1, the upper atmosphere (>~75km) is oxic, and the deeper atmosphere (20-75km) is nearly neutral ($CO/O_2 \approx 2$). The oxygen concentration high in the top layer of the atmosphere but decreases rapidly with decreasing altitude. The photolysis of CO_2 occurs predominantly in the lower layers (~75 km, varies with different initial atmospheric CO_2) because CO_2 is not stable higher

194 in the atmosphere. At these altitudes where CO_2 is photolyzed, the atmosphere should
195 not be more oxidizing than CO_2 (Zahnle and Buick, 2016). However, the lighter atom
196 (O) has a larger transmission efficiency than the heavier molecule (CO). Therefore, O
197 can exceed CO in the upper atmosphere (above ~75km). Thus, O and CO are produced
198 in the lower layers (~75km), but the higher transmission efficiency of O than CO means
199 that it accumulates in the upper atmosphere to form an oxic environment. The results
200 in Payne et al. (2020) combined with this study provide strong evidence for such a
201 mechanism.
202 Figure 2 shows the MOMIP results of iron particles with 5μm-radius. Various initial
203 velocity (12-20km/s) and three different downward angles (the MMs velocity angle at
204 the top of atmosphere): 0° (vertical), 45°,85° (near horizontal) are considered. The solid
205 curves represent the O to Fe atoms ratio ($Ratio_{O:Fe}$) in the simulated particles. It should
206 be noted that the peak temperature of particles with a downward angle >85° does not
207 reach the melting point of iron, which means these particles cannot quench-crystalize
208 to form MMs of interlocking dendritic crystals during their trajectories. Therefore, we
209 show the results of 0° (vertical, the left four panels, Panel A, D, G, J of Figure 2), 45°
210 (the middle four panels, Panle B, E, H, K of Figure 2), and 85° (nearly horizontal, the
211 right four panels, Panel C, F, I, L of Figure 2) downward trajectories. The particle
212 captures negligible O_2 when it enters the troposphere (tropopause at 20km) because its
213 velocity is slow (<5 m/s) and O_2 concentrations are deficient here. Therefore, we only
214 present the results above 20km. The 0° (vertical) downward particles have a greater
215 $Ratio_{O:Fe}$ compared to 45° and 85° (nearly horizontal) downward trajectories. This is

because the vertical downward particles fall faster and collide with air molecules with greater velocity, thus having higher temperatures, faster reaction rates, and greater Ratio_O:Fe.

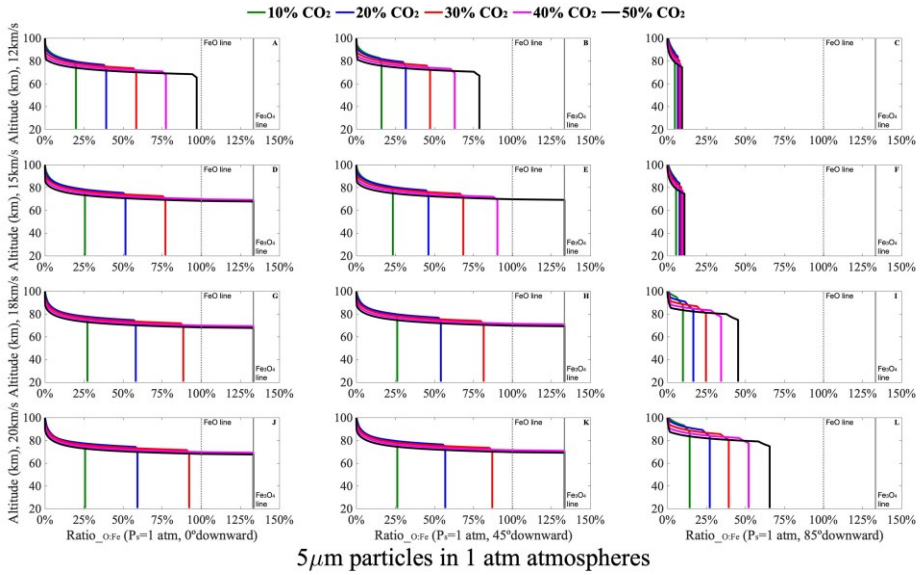

Figure 2. The MOMIP model results of 5μm-radius iron particles with fCO_2 ranging from 10% to 50%. The vertical represents altitude, and the horizontal axis represents Ratio_O:Fe. Three different downward angles are simulated: 0° (vertically, the left four panels), 45° (the middle four panels), and 85° (nearly horizontally, the right four panels). Four different initial velocities (12, 15, 18, and 20 km/s) are presented up to the bottom. The vertical grey dashed lines in Figure 2 represents Ratio_O:Fe in FeO which is 1:1 or 100% while the vertical black solid lines represent Ratio_O:Fe in Fe_3O_4, 4:3 or 133.3%.

No green, blue, and red curve (corresponding to cases with $fCO_2 \leq 30\%$) in Figure 2 reaches the vertical black solid line, suggesting that an atmosphere with fCO_2 below 30% is unable to oxidize the 5μm-radius MMs to Fe3O4-only state fully. In contrast, the pink and black curves of Figure 2D, G, J, H, K (corresponding to cases with $fCO_2 \geq$~40% and different velocities and downward angles) touch the vertical black solid line (Ratio_O:Fe in Fe_3O_4), suggesting that atmospheres with fCO_2 >30% are required to produce Fe_3O_4-only 5μm-radius MMs as found in Tomkins et al. (2016).

Generally, larger iron particles require more oxidants to become oxidized. However, our simulations show that smaller particles, rather than the larger MMs, require higher

atmospheric oxidant content (see the supplementary Figure S1-S2) because smaller particles have lower peak temperatures resulting in slower reaction rate constants during their trajectories. This is also presented in the Figure 2 of Tomkins et al. (2016). Hence, smaller MMs could constrain the lower limit of atmospheric CO_2 content. To further constrain the fCO_2 2.7 billion years ago, we performed simulations with initial CO_2 content between 30% and 40% (see Figure 3 for results).

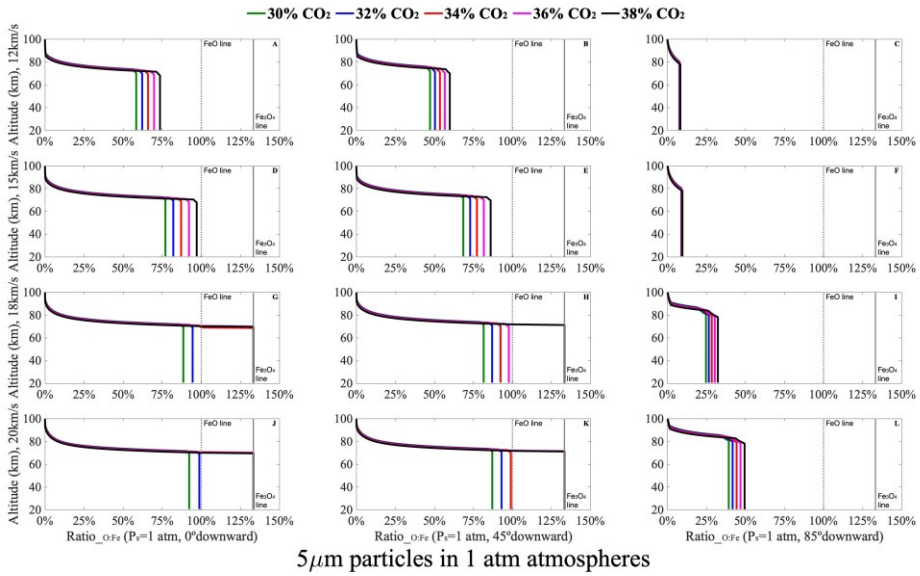

Figure 3. The MOMIP model results of 5μm-radius iron particles with fCO_2 ranging from 30% to 38%.

Figure 3G and 3J show that Fe_3O_4-only MMs cannot be produced when the initial fCO_2 is lower than 32%. Therefore, the results suggest fCO_2 >32% at 2.7 Ga. We should also note that when fCO_2 is >32%, particles with larger downward angles (the right column of Figure 3) or slower velocities (the upper six panels of Figure 3) do not reach the vertical grey dashed line, meaning the particles' compositions in these cases are Fe-FeO mixed, the other type of MMs found by Tomkins et al. (2016). Hence, all the Fe_3O_4-only and Fe-FeO mixed MMs with the radius of 5-25 μm found by Tomkins et al. (2016) are predicted in our model when fCO_2 >32%. Therefore, MMs found by

Tomkins et al. (2016) suggest an atmosphere with fCO_2 >32% at 2.7 Ga.

DISCUSSION

Inferences of very high CO_2 imply a warm Late Archean climate and raise questions of consistency with the chemistry of paleosols deposited near 2.7 Ga (Payne et al., 2020), as well as with climate proxies. Since the 'Faint Young Sun Paradox' (FYSP) was proposed (Sagan and Mullen, 1972), what kept the Earth warm during the Archean has been continuously debated. The greenhouse effect of ammonia, methane, CO_2, and the collision-induced absorption of nitrogen and hydrogen have all been considered as potential solutions to the FYSP in different studies (Haqq-Misra et al., 2008; Kasting, 1987; Sagan and Mullen, 1972). However, ammonia is unstable against photolysis (Kuhn and Atreya, 1979), and methane would cause organic haze at high concentration (Arney et al., 2016; Haqq-Misra et al., 2008; Pavlov et al., 2000) which has an anti-greenhouse effect. Hence CO_2 remains the most plausible option for the primary greenhouse gas.

Kasting (1987) originally suggested that 100-1000 times the present atmospheric level (PAL, taken as 340ppmv in Kasting, 1987) of CO_2, i.e. 0.034-0.34 atm (if other species adjust to maintain constant atmospheric pressure), is needed to solve the FYSP at 2.5 Ga. But early work suggested ancient paleosols would be expected to contain siderite (iron carbonate) at depth if CO_2 were so abundant, and its absence led to inferences of CO_2 <100 PAL, i.e. <0.034 atm (Rye et al., 1995). Subsequent paleosol modelling estimated CO_2 ~10-50 PAL (0.0034-0.017 atm) at ~2.7 Ga (Driese et al., 2011; Sheldon, 2006). But due to limitations of the method, CO_2 content results reconstructed from

paleosols are criticized. Payne et al. (2020) pointed out that the assumption applied in Sheldon (2006) is problematic, in which silicate minerals were assumed to react with every CO_2 molecule that enters the soil from the atmosphere. Thus it is suggested that CO_2 content constrained from paleosols should only be interpreted as a lower limit (Payne et al., 2020). Likewise, Wang and Shen (2019), via applying an ocean-atmosphere coupling model, proposed that atmospheric CO_2 content was not the only determining factor for siderite precipitation in paleosols. Therefore the absence of siderite in Archean paleosols may not be a constraint for low Archean atmospheric CO_2 content (Wang and Shen, 2019). Additionally, more sophisticated paleosol modelling gives estimates of CO_2 ~85-510 PAL (0.029-0.17 atm) at ~2.77 Ga and ~78-2500 PAL (0.027-0.85 atm) at ~2.75 Ga (Kanzaki and Murakami, 2015). Overall, our minimum CO_2 estimate at 2.7 Ga from MMs oxidation, fCO_2>32% (~941 PAL, 0.32 atm), is not incompatible with the paleosols results.

However, our CO_2 estimate is higher than the value needed to solve the FYSP (Kasting, 1987), implying a warm Late Archean climate. Payne et al. (2020) suggested that fCO_2 >25% combined with 0.8-atm N_2 would cause the mean surface temperature to exceed 300K at 2.7 Ga. They note this is inconsistent with interpreted glacial diamictites at ~2.7 Ga (Ojakangas et al., 2014) and with more convincing evidence of glaciation 200 Myr earlier at ~2.9 Ga (Young et al., 1998). Therefore, Payne et al. (2020) argue for lower N_2 pressure to cool the surface at ~2.7 Ga, which has some independent support (Catling and Zahnle, 2020). However, there is a long-running debate over Archean temperatures, which conceivably varied considerably over geologic timescales,

297 just as they have in the Phanerozoic. Oxygen isotope data from cherts has been used to
298 infer Archean ocean temperatures as high as 358K (Knauth and Lowe, 2003), but the
299 reliability of the proxy is questioned (Catling and Zahnle, 2020), and other isotope
300 proxies give estimates <313K (Hren et al., 2009) or <308K (Blake et al., 2010). Given
301 this uncertainty, the partial pressure of CO_2 >0.32 atm at ~2.7 Ga and associated
302 warming implied by our results seems plausible, and the need to invoke lower surface
303 pressure at the time hinges on whether compelling evidence of glaciation exists near
304 synchronous with the micrometeorite deposits.
305 The simulations here modeled the oxidation of iron particles that entered the Archean
306 atmosphere under different initial atmospheric CO_2 concentrations, suggesting that the
307 oxidation path by either CO_2 or O_2 alone cannot explain the observed Fe_3O_4-only MMs
308 in Tomkins et al. (2016). Combining the oxidant power of CO_2 and O_2, the observed
309 MMs could form in an atmosphere with >32% CO_2, suggesting comparable conditions
310 in the late-Archean atmosphere. If this interpretation is correct, it also readily solves
311 the Faint Young Sun Paradox at ~2.7 Ga, suggesting a warm-hot Late Archean unless
312 atmospheric pressure was markedly reduced.
313 **ACKNOWLEDGMENTS**
314 G.H would like to thank sponsorship from China Scholarship Council. G.H thanks Prof. Feng
315 Tian for introducing the photochemical model and the Earth's early atmosphere. G.H also
316 thanks Q.T for the help during the revision. J.K.E would like to thank the Hill Family
317 Scholarship generously supported by University of Exeter alumnus and president of the
318 University's US Foundation Graham Hill (Economic & Political Development, 1992) and other

donors to the US Foundation. This work was partly supported by a Science and Technology Facilities Council Consolidated Grant (ST/R000395/1). N.J.M. was supported by a UKRI Future Leaders Fellowship: MR/T040866/1. T.M.L. was supported by NERC (NE/P013651/1).

AUTHOR CONTRIBUTIONS

G.H developed the atmospheric entry model and modified the photochemical model, performed simulations and data analysis, and wrote the manuscript. T.M.L provided insight on the atmospheric entry model and the photochemical model, helped data analysis and wrote the manuscript. J.K.E helped data analysis and improved the manuscript. N.J.M provided suggestions on modifying models, helped data analysis, and improved the manuscript. D.C improved the manuscript. J.M, E.H, and Z.L provided insight.

REFERENCES CITED

Abuluwefa, H., Guthrie, R., Ajersch, F., 1997. Oxidation of low carbon steel in multicomponent gases: Part I. Reaction mechanisms during isothermal oxidation. Metallurgical and Materials Transactions A 28, 1633-1641.

Arney, G., Domagal-Goldman, S.D., Meadows, V.S., Wolf, E.T., Schwieterman, E., Charnay, B., Claire, M., Hébrard, E., Trainer, M.G., 2016. The pale orange dot: the spectrum and habitability of hazy Archean Earth. Astrobiology 16, 873-899.

Blake, R.E., Chang, S.J., Lepland, A., 2010. Phosphate oxygen isotopic evidence for a temperate and biologically active Archaean ocean. Nature 464, 1029-1032.

Catling, D.C., Zahnle, K.J., 2020. The Archean atmosphere. Science Advances 6, eaax1420.

Cloud, P., 1972. A working model of the primitive Earth. American Journal of Science

341 272, 537-548.
342 Corbari, R., Fruehan, R., 2010. Reduction of iron oxide fines to wustite with CO/CO 2
343 gas of low reducing potential. Metallurgical and Materials transactions B 41, 318-329.
344 Driese, S.G., Jirsa, M.A., Ren, M., Brantley, S.L., Sheldon, N.D., Parker, D., Schmitz,
345 M., 2011. Neoarchean paleoweathering of tonalite and metabasalt: Implications for
346 reconstructions of 2.69 Ga early terrestrial ecosystems and paleoatmospheric chemistry.
347 Precambrian Research 189, 1-17.
348 Farquhar, J., Bao, H., Thiemens, M., 2000. Atmospheric influence of Earth's earliest
349 sulfur cycle. Science 289, 756-758.
350 Garnaud, G., Rapp, R.A., 1977. Thickness of the oxide layers formed during the
351 oxidation of iron. Oxidation of Metals 11, 193-198.
352 Genge, M.J., 2016. The origins of I-type spherules and the atmospheric entry of iron
353 micrometeoroids. Meteoritics & Planetary Science 51, 1063-1081.
354 Gregory, B.S., Claire, M.W., Rugheimer, S., 2021. Photochemical modelling of
355 atmospheric oxygen levels confirms two stable states. Earth and Planetary Science
356 Letters 561, 116818.
357 Haqq-Misra, J.D., Domagal-Goldman, S.D., Kasting, P.J., Kasting, J.F., 2008. A
358 revised, hazy methane greenhouse for the Archean Earth. Astrobiology 8, 1127-1137.
359 Himmel, L., Mehl, R., Birchenall, C.E., 1953. Self-diffusion of iron in iron oxides and
360 the Wagner theory of oxidation. JOM 5, 827-843.
361 Hren, M., Tice, M., Chamberlain, C., 2009. Oxygen and hydrogen isotope evidence for
362 a temperate climate 3.42 billion years ago. Nature 462, 205-208.

363 Kanzaki, Y., Murakami, T., 2015. Estimates of atmospheric CO2 in the Neoarchean–
364 Paleoproterozoic from paleosols. Geochimica et Cosmochimica Acta 159, 190-219.
365 Kasting, J., Donahue, T., 1980. The evolution of atmospheric ozone. Journal of
366 Geophysical Research: Oceans 85, 3255-3263.
367 Kasting, J.F., 1987. Theoretical constraints on oxygen and carbon dioxide
368 concentrations in the Precambrian atmosphere. Precambrian research 34, 205-229.
369 Kasting, J.F., 1993. Earth's early atmosphere. Science 259, 920-926.
370 Kasting, J.F., Liu, S., Donahue, T., 1979. Oxygen levels in the prebiological atmosphere.
371 Journal of Geophysical Research: Oceans 84, 3097-3107.
372 Kasting, J.F., Zahnle, K.J., Walker, J.C., 1983. Photochemistry of methane in the
373 Earth's early atmosphere. Precambrian Research 20, 121-148.
374 Knauth, L.P., Lowe, D.R., 2003. High Archean climatic temperature inferred from
375 oxygen isotope geochemistry of cherts in the 3.5 Ga Swaziland Supergroup, South
376 Africa. Geological Society of America Bulletin 115, 566-580.
377 Kuhn, W.R., Atreya, S.K., 1979. Ammonia photolysis and the greenhouse effect in the
378 primordial atmosphere of the Earth. Icarus 37, 207-213.
379 Lehmer, O., Catling, D., Buick, R., Brownlee, D., Newport, S., 2020. Atmospheric CO2
380 levels from 2.7 billion years ago inferred from micrometeorite oxidation. Science
381 advances 6, eaay4644.
382 Love, S., Brownlee, D., 1991. Heating and thermal transformation of micrometeoroids
383 entering the Earth's atmosphere. Icarus 89, 26-43.
384 Ohmoto, H., 1996. Evidence in pre–2.2 Ga paleosols for the early evolution of

385 atmospheric oxygen and terrestrial biota. Geology 24, 1135-1138.
386 Ojakangas, R.W., Srinivasan, R., Hegde, V., Chandrakant, S., Srikantia, S., 2014. The
387 Talya conglomerate: An Archean (~ 2.7 Ga) glaciomarine formation, Western Dharwar
388 Craton, Southern India. Current Science, 387-396.
389 Pavlov, A., Kasting, J., 2002. Mass-independent fractionation of sulfur isotopes in
390 Archean sediments: strong evidence for an anoxic Archean atmosphere. Astrobiology
391 2, 27-41.
392 Pavlov, A.A., Brown, L.L., Kasting, J.F., 2001. UV shielding of NH3 and O2 by
393 organic hazes in the Archean atmosphere. Journal of Geophysical Research: Planets
394 106, 23267-23287.
395 Pavlov, A.A., Kasting, J.F., Brown, L.L., Rages, K.A., Freedman, R., 2000.
396 Greenhouse warming by CH4 in the atmosphere of early Earth. Journal of Geophysical
397 Research: Planets 105, 11981-11990.
398 Payne, R.C., Brownlee, D., Kasting, J.F., 2020. Oxidized micrometeorites suggest
399 either high pCO2 or low pN2 during the Neoarchean. Proceedings of the National
400 Academy of Sciences 117, 1360-1366.
401 Ribas, I., Guinan, E.F., Güdel, M., Audard, M., 2005. Evolution of the solar activity
402 over time and effects on planetary atmospheres. I. High-energy irradiances (1-1700 Å).
403 The Astrophysical Journal 622, 680.
404 Rye, R., Kuo, P.H., Holland, H.D., 1995. Atmospheric carbon dioxide concentrations
405 before 2.2 billion years ago. Nature 378, 603-605.
406 Sagan, C., Mullen, G., 1972. Earth and Mars: Evolution of atmospheres and surface

temperatures. Science 177, 52-56.

Shao, H., Isobe, H., Miao, B., 2020. Reproduction of I-type cosmic spherules and characterization in an Fe-Ni-O system. Meteoritics & Planetary Science 55, 2066-2079.

Sheldon, N.D., 2006. Precambrian paleosols and atmospheric CO2 levels. Precambrian Research 147, 148-155.

Smirnov, V., 2008. Rate constant of the gas-phase reaction between Fe atoms and CO 2. Kinetics and Catalysis 49, 607-609.

Tomkins, A.G., Bowlt, L., Genge, M., Wilson, S.A., Brand, H.E., Wykes, J.L., 2016. Ancient micrometeorites suggestive of an oxygen-rich Archaean upper atmosphere. Nature 533, 235.

Vicentini, E.D., de Lima Batista, A.P., de Oliveira-Filho, A.G.S., 2020. Computational mechanistic investigation of the Fe+ CO 2→ FeO+ CO reaction. Physical Chemistry Chemical Physics 22, 16943-16948.

Wang, R., Shen, B., 2019. Snowball Earth at low solar luminosity prevented by the ocean–atmosphere coupling. Acta Geochimica 38, 775-784.

Young, D.J., 2008. High temperature oxidation and corrosion of metals. Elsevier.

Young, G.M., Brunn, V.V., Gold, D.J., Minter, W., 1998. Earth's oldest reported glaciation: physical and chemical evidence from the Archean Mozaan Group (∼ 2.9 Ga) of South Africa. The Journal of Geology 106, 523-538.

Zahnle, K., Buick, R., 2016. Atmospheric science: Ancient air caught by shooting stars. Nature 533, 184-186.

Zahnle, K., Claire, M., Catling, D., 2006. The loss of mass-independent fractionation

in sulfur due to a Palaeoproterozoic collapse of atmospheric methane. Geobiology 4, 271-283.

Zahnle, K.J., 1986. Photochemistry of methane and the formation of hydrocyanic acid (HCN) in the Earth's early atmosphere. Journal of Geophysical Research: Atmospheres 91, 2819-2834.

Zerkle, A.L., Claire, M.W., Domagal-Goldman, S.D., Farquhar, J., Poulton, S.W., 2012. A bistable organic-rich atmosphere on the Neoarchaean Earth. Nature Geoscience 5, 359-363.

Supplementary Materials for "CO_2 and O_2 oxidised 2.7 Ga micrometeorites in two stages suggesting a >32% CO_2 atmosphere"

G. Huang[1,2]*, J. K. Eager[3], N. J. Mayne[3], D. Cui[1], J. Manners[2,4], E. Hebrard[3], Z. Liu[1], and T. M. Lenton[2]

*Corresponding author. Email: hg17@mails.tsinghua.edu.cn;

SUPPLEMENTARY FIGURES

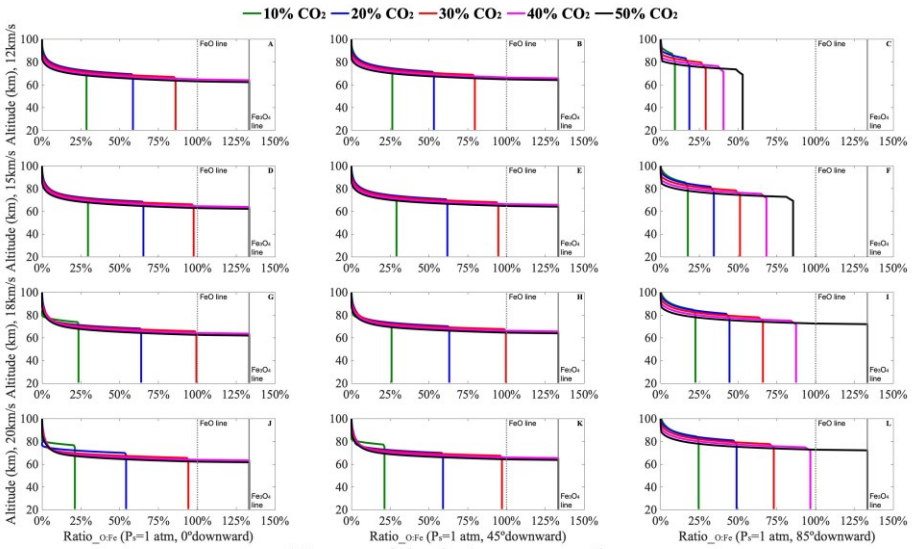

Figure S1. Results of the MOMIP model with 15-μm radius, fCO_2 ranging from 10% to 50%. The vertical represents altitude, and the horizontal axis represents $Ratio_{\_O:Fe}$. Three different downward angles are simulated: 0° (vertically, the left four panels), 45° (the middle four panels), and 85° (nearly horizontally, the right four panels). Four different initial velocities (12, 15, 18, and 20 km/s) are presented up to the bottom. The vertical grey dashed lines in Fig. 2 represents $Ratio_{\_O:Fe}$ in FeO which is 1:1 or 100% while the vertical black solid lines represents $Ratio_{\_O:Fe}$ in Fe_3O_4, 4:3 or 133.3%.

453

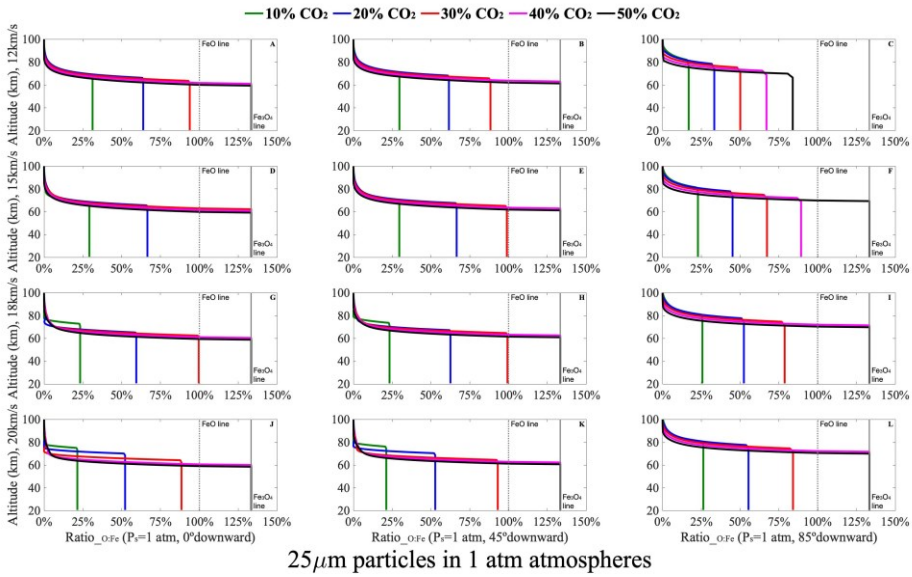

454

455 Figure S2. Results of the MOMIP model with 25-μm radius, fCO_2 ranging from 10%

456 to 50%.

457

458